Sustainable and Practical Superhydrophobic Surfaces via Mechanochemical Grafting

Nusret Celik, Serdar Akay, Furkan Sahin, Gulay Sezer, Esen Dagasan Bulucu, Mahmut Ruzi, Hans-Jürgen Butt,* and Mustafa Serdar Onses*

The broad adoption of superhydrophobic surfaces in practical applications is hindered by limitations of existing methods in terms of excessive usage of solvents, the need for tedious and lengthy chemical processes, insufficient biocompatibility, and the high cost of materials. Herein, a mechanochemical approach for practical and solvent-free manufacturing of superhydrophobic surfaces is reported. This approach enables solvent-free and ultra-rapid preparation of superhydrophobic surfaces in a single-step without the need for any washing, separation, and drying steps. The hydrolytic rupture of siloxane bonds and generation of free radicals induced by mechanochemical pathways play a key role in covalent grafting of silicone to the surface of nanoparticles that leads to superhydrophobic surfaces with a water contact angle of >165° and a sliding angle of <2°. The direct use of industrially available and non-functional silicone materials together with demonstrated applicability to inorganic nanoparticles of varied composition greatly contribute to the scalability of the presented approach. The resulting superhydrophobic surfaces are highly biocompatible as demonstrated by fibroblast cells using two different assays. Monolith materials fabricated from silicone-grafted nanoparticles exhibit bulk and durable superhydrophobicity. The presented approach offers tremendous potential with sustainability, scalability, cost-effectiveness, simplicity, biocompatibility, and universality.

1. Introduction

Superhydrophobic surfaces show extreme repellency and low adhesion to water. Droplets on such surfaces display large contact angle (>150°) and readily roll off at low sliding angles.[1–3] Popularized by the discovery and elucidation of self-cleaning mechanism of lotus leaves,[4,5] superhydrophobic surfaces have attracted significant attention for practical applications such as self-cleaning solar cells,[6–8] corrosion inhibition layers on metal surfaces,[9,10] anti-icing coatings,[11,12] and oil/water separation membranes and meshes.[13–15] Superhydrophobic surfaces have been adopted in a number of niche applications such as blood-repellent garments,[16] anti-biofouling coatings,[17,18] and to concentrate molecules for bio-assay analysis and increase detection limit.[19,20] Superhydrophobic surfaces feature heterogeneous morphology with nanoscopic and microscopic roughness in the form of protrusions separated by air pockets and are generally fabricated by using low surface energy materials.[21] The combination of nano/micro-scale protrusions with low surface energy leads to diminished adhesion and improved droplet mobility.

The excessive usage of solvents and toxic chemicals, long and tedious chemical processes, limited biocompatibility, and costly materials are challenges in the sustainable fabrication of superhydrophobic surfaces. A convenient and universal method, also adapted in commercial

N. Celik, F. Sahin, M. Ruzi, M. S. Onses
ERNAM – Erciyes University Nanotechnology Application and Research Center
Kayseri 38039, Turkey
E-mail: onses@erciyes.edu.tr
N. Celik, S. Akay, E. Dagasan Bulucu, M. S. Onses
Department of Materials Science and Engineering
Erciyes University
Kayseri 38039, Turkey

G. Sezer
Department of Pharmacology
Erciyes University
Faculty of Medicine
Kayseri 38039, Turkey
H.-J. Butt
Max Planck Institute for Polymer Research
D-55128, Mainz, Germany
E-mail: butt@mpip-mainz.mpg.de
M. S. Onses
UNAM–National Nanotechnology Research Center
Institute of Materials Science and Nanotechnology
Bilkent University
Ankara 06800, Turkey

products, is the deposition of colloidal dispersions of nanoparticles functionalized or mixed with hydrophobic molecules.[22,23] The preparation of such colloidal dispersions is typically performed in organic solvents through functionalization with hydrophobic molecules such as alkylsilanes or perfluoroalkylsilanes. These functionalization steps are often accompanied with additional washing and dryings steps. The entire process takes on the order of several hours/days and requires excessive usage of organic solvents. For example, hexane, a solvent used in some studies,[24,25] is highly flammable, can cause skin and respiratory organ irritation if exposed, and is toxic to aquatic life. The major issue, though, is waste and emission of volatile organic compounds: since colloidal coating solution is dilute. The increasing consumer consciousness about the environment and personal health, followed by progressively stringent regulations are compelling to reduce or completely eliminate hazardous processes and harmful or polluting chemicals, such as flammable and toxic organic solvents.[26,27] The excess usage of solvent and wet chemical processes challenge scaling up of the processes and wide adaption of the superhydrophobic materials by researchers with limited wet-chemistry experience.

Solvent-free fabrication, though formidable, can be a rewarding approach. The deposition of soot and carbonaceous particles via flame synthesis and thermal processing is one method to fabricate superhydrophobic surfaces without use of solvents.[6,28,29] Laser or plasma treatment followed by deposition of hydrophobic coatings is another strategy.[30] Imparting surface roughness to hydrophobic polymers via hot-pressing, mechanical wrinkling, or gas bubbles while curing polymers also result in superhydrophobicity.[31–33] Notwithstanding the efforts, superhydrophobic coatings and surfaces that have been fabricated via solvent-free methods so far involve either heat treatment or usage of toxic and corrosive chemicals.

Here, we present all dry fabrication of superhydrophobic surfaces through mechanochemical grafting of silicone. The entire process consists of agitating silicone and nanoparticles in a planetary ball mill for a duration on the order of minutes. A low-cost and biocompatible silicone is employed for lowering the surface energy of nanoparticles. Silicone is liquid at room temperature and does not possess reactive groups. Mechanochemical approaches[34–36] enable solventless chemical modification of particulate materials with practical utility demonstrated for applications other than superhydrophobic coatings. In the present study, we show that the agitation in the ball milling process results in covalent grafting of non-functional and low-cost silicone, methyl terminated poly(dimethylsiloxane) to the surface of metal oxide nanoparticles. A minimal chain length of silicone is required above which superhydrophobicity is attained. Mechanistic studies are performed to study the origin of grafting non-functional silicone. A key advantage of the presented approach is solvent-free fabrication of superhydrophobic materials in durations as short as 5 min without need for washing, separation, and drying steps. The fabricated superhydrophobic surfaces are biocompatible as demonstrated by two assays via fibroblast cells. We finally demonstrate solvent-free preparation of bulk and durable superhydrophobic materials using silicone grafted silica nanoparticles.

2. Results and Discussion

2.1. Mechanochemical Fabrication of Superhydrophobic Surfaces

To fabricate superhydrophobic surfaces, the process starts with direct mixing of silicone (1 g, 63 000 g mol^{-1}) and silica nanoparticles (2 g), without any pre-treatment (**Figure 1**a; Video S1, Supporting Information). Specifically, methyl terminated poly(dimethylsiloxane) (Me-PDMS) is used as the silicone, which is commonly referred as silicone oil (Figure 1a). Herein, silicone is simply mixed with powdered nanoparticles without the use of any additional cross-linking agents. The grafting of silicone to the nanoparticles is achieved by using a planetary ball mill. During the ball milling, collisions between tungsten carbide balls and walls of the chamber result in hydrolytic rupture of siloxane bonds and mechanochemical generation of free radicals in the silicone, which grafts to the surface of nanoparticles. After a milling time as short as 5 min, the superhydrophobic powder was obtained. The powder was retrieved using a spatula and placed evenly on a flat surface with the aid of a glass slide, on which a water droplet (10 µL) beads up with water CA of 165° and sliding angle of <2°. The water repellency can be further increased at longer milling times. It should be noted that the superhydrophobic powder can be easily dispersed in common organic solvents such as acetone if needed and can be spray coated to obtain a thin homogeneous superhydrophobic layer (Video S2, Supporting Information).

The mechanochemical grafting of silicone provides key advantages in terms of the water repellency and duration of the preparation process. The grafting of Me-PDMS to surfaces terminated with silicon oxide is known from previous studies.[37,38] This grafting is simply performed by dropping silicone on the substrate of interest for long durations (e.g., 24 h). To see the effect of the mechanochemical process on the grafting of silicone, silica nanoparticles were modified with Me-PDMS using three methods. In addition to the ball milling, silica nanoparticles and silicone were simply mixed without any agitation at room temperature and 100 °C for 30 min and 24 h. All materials were subjected to repeated washing in toluene to ensure removal of ungrafted silicone. Figure 1b,c shows the significant contrast in the wetting properties of materials prepared by these three different methods. The superhydrophobic powder was obtained after 30 min of ball milling at 200 rpm with a water CA 168° and SA 2°. In the absence of ball milling, the particles treated with silicone for 30 min exhibited hydrophilic behavior (CA<10°). Even increasing the temperature of the treatment to 100 °C did not improve the hydrophobicity for unmilled samples. Increasing the duration of the treatment to 24 h improved the hydrophobicity with water CAs of 137° and 143° for unmilled samples grafted at room temperature and 100 °C, respectively. The SAs were higher than 30° showing the limited liquid repellency of these unmilled particles. These results demonstrate the advantages of the mechanochemical grafting. The SHP materials can be prepared in short durations of time with notably high-water repellence. This mechanochemical grafting of silicone appears to be universal as demonstrated with particles of other oxides such as titanium dioxide,
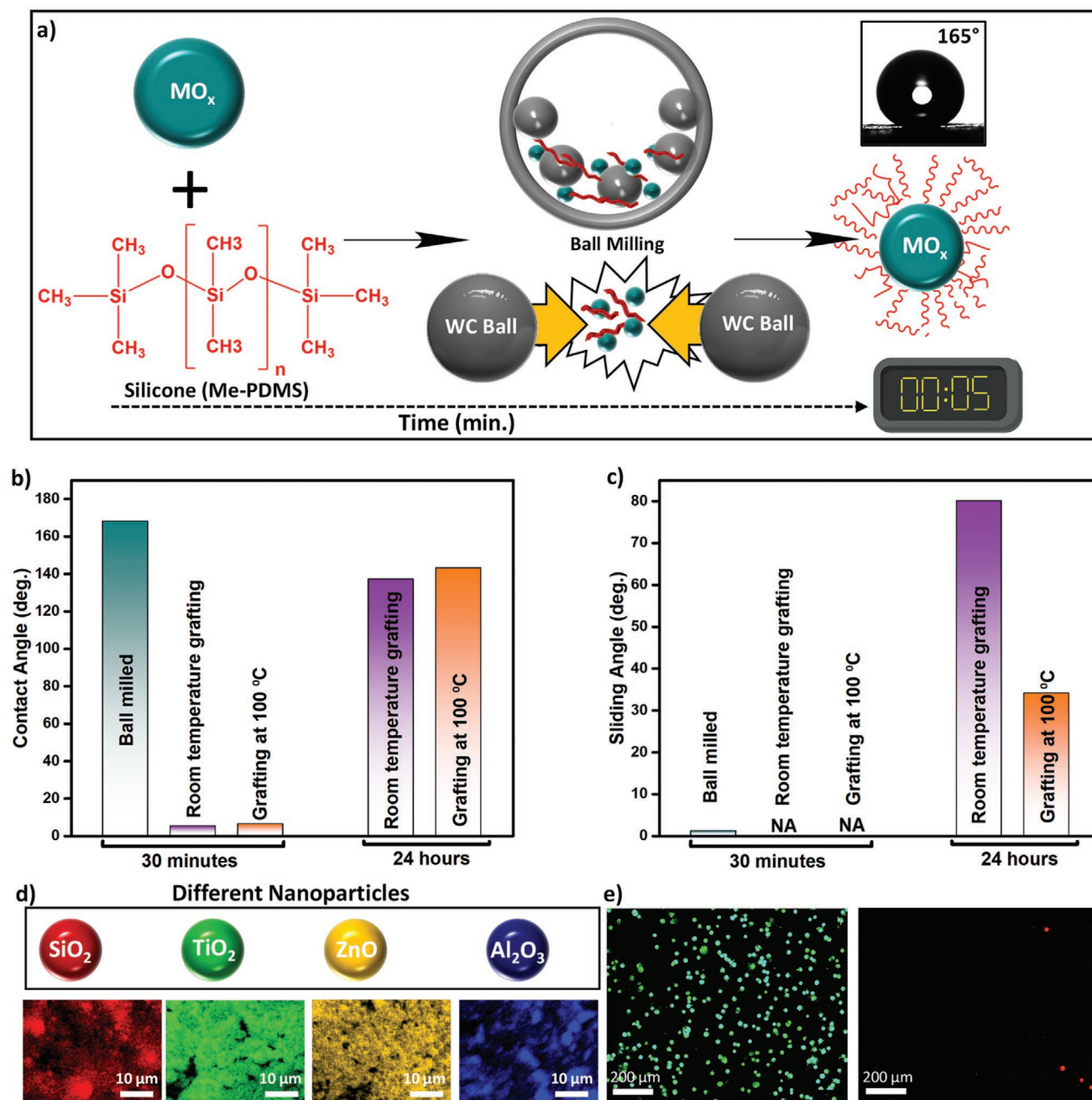
Figure 1. Mechanochemical fabrication of superhydrophobic surfaces. a) Schematic illustration of the process. MOx represents inorganic oxide particles such as SiO_2, TiO_2, ZnO, and Al_2O_3. The superhydrophobic surfaces can be obtained in 5 min by ball milling at 300 rpm. b,c) Effect of grafting conditions on CA (b) and SA (c) of a water droplet (10 μL) on the obtained powder prepared via ball milling at 200 rpm for 30 min, unmilled grafting at room temperature and unmilled grafting at 100 °C for 30 min and 24 h, respectively. NA: the droplet sticks to the surface and does not roll off. d) Grafting of silicone onto various nanoparticles, showing the EDX mapping image. e) fluorescence microscope image of the stained cells. Live cells appear green and dead cells appear red. The size of SiO_2 particles is 11 nm in diameter and the molecular weight of the silicone is 63 000 g mol^{-1}.

zinc oxide, as well as aluminum oxide (Figure 1d; Figure S1, Supporting Information).

An additional consideration for superhydrophobic coatings is the biocompatibility of the materials. This aspect is particularly important for applications such as medical and microfluid devices.[39,40] Silicone is widely considered as a biocompatible

material. To qualitatively assess the biocompatibility of silicone grafted silica NPs, we performed several different tests. First, the cytotoxicity of the superhydrophobic powder was analyzed via the MTT assay, which can probe mitochondrial NADPH metabolic activation. Cells cultured with different concentrations of superhydrophobic powder had a mean viability of

97.8 ± 2% compared to cell lines cultured with the complete medium (Figure S2, Supporting Information). The results showed that the sample extracts exhibited high biocompatibility against L929 fibroblast cells ($p > 0.05$). Furthermore, the cell viability was assessed by staining with SYTO9 and PI, which emit green and red fluorescence, respectively. SYTO9 selectively binds to nucleic acids of live eukaryotic/prokaryotic cells, whereas PI only permeates to dead/damaged cells.[41] Figure 1e shows representative fluorescence microscopy images of the stained cells cultured on the superhydrophobic powders. More than 98% of the cells was live as indicated by the strong green fluorescence. The mean cell viability calculated from the fluorescence microscope images was 101.4 ± 0.3% relative to the control surface, in agreement with the MTT results (Table S1, Supporting Information). These results show strong promise of the proposed materials in a broad range of applications in biomedical devices, food-packaging, and wearable electronics where the biocompatibility is important. Further experiments and systematic investigations probing the long-term effects are needed before direct use in such applications.

2.2. Effects of Processing Parameters on the Superhydrophobicity

The mechanochemical processing time and grinding speed, relative amount of silicone with respect to the surface area of powdered nanoparticles, the chain length of silicone and size of nanoparticles play important roles in the mechanochemical fabrication of superhydrophobic surfaces. **Figure 2** presents the surface wetting properties of the obtained powder as a function of these parameters. As shown in Figure 2a, when grinded for 30 min at a low (100 rpm) speed, the contact angle is <120°. However, when the grinding speed is 150 rpm and above, the powder shows superhydrophobic properties, where the contact angle becomes higher than 150° and the sliding angle is <10° (Figure 2a). Therefore, a grinding speed of 200 rpm is chosen to prepare superhydrophobic powders unless stated otherwise. The grinding time also impacts the hydrophobicity of the obtained powder. When grinded at 200 rpm for a short duration (15 min), the resultant powder exhibits water CA of 160° but water droplets pin on the surface (SA>10°). When the grinding time in the ball milling was 30 min, the water CA increased to 168° and SA decreased to 2°. Further increasing milling time to 60 min results in a slight increase of water CA and slight decrease of SA. Beyond 60 min, the grinding time in ball milling does not lead to noticeable change on the wetting property (Figure 2b). Furthermore, there is a close relationship between the grinding speed and grinding time needed to obtain superhydrophobicity. When the grinding speed is increased to 300 rpm, the superhydrophobic powder with a water CA of 165° and SA of 1° is obtained in a short time (5 min) (Figure 2c). This result shows that the grafting time can be reduced at high grinding speeds.

An important parameter is the ratio of the amount of silicone oil to the total surface area (m^2), obtained by multiplying the mass of silica NPs by the specific surface area, of the powdered nanoparticles. Figure 2d presents the variation of contact angle of the obtained powder as a function of this ratio for two different sizes of nanoparticles. The amount of silicone was varied as 0.5, 1.0, 1.25, 1.5, and 2.0 g while the mass of silica particles was kept as 2.0 g for silica particles of two different diameters and specific surface areas (≈186 $m^2 g^{-1}$ for 11 nm and 175 $m^2 g^{-1}$ for 90 nm). When there are enough silicone molecules to cover the entire NP surface, the resultant powder becomes superhydrophobic. However, further increasing the amount of silicone results in reduced hydrophobicity where the obtained powder is no longer superhydrophobic, and in pellet form instead of powder. Figure 2d implies that a superhydrophobic powder can be obtained when the ratio of silicone mass to the total surface area of silica nanoparticles is <0.003 $g m^{-2}$. Thus, the mass ratio of 1:2 (1 g silicone: 2 g silica) is optimal for obtaining a superhydrophobic powder for both 11 nm diameter (0.0027 $g m^{-2}$) and 90 nm diameter (0.0029 $g m^{-2}$) silica nanoparticles. The specific surface areas of two different sizes of nanoparticles are close due to the powdered nature and polydispersity of materials. When silicone is in excess, some molecules can fill in the gaps between the particles by replacing air pockets, leading to decrease of surface roughness and thus CA. However, upon washing with toluene, the pellet takes powder form and now exhibits superhydrophobicity (Figure S3, Supporting Information). The FTIR spectrum confirmed a decrease of silicone peaks after washing but not complete disappearance.

The molecular weight of silicone is another important parameter. Figure 2e presents the variation of surface wetting properties of the surfaces prepared by using different molecular weights of silicone. The CA increased and the SA decreased with increasing silicone molecular weight. At least 6000 $g mol^{-1}$ was needed to achieve superhydrophobicity (CA = 168°, SA = 4°). Then, at a molecular weight of ≈63 000 $g mol^{-1}$, both the CA and SA values saturated at a value of 172° and 1°, respectively. These results suggest a certain chain length that is necessary to achieve superhydrophobicity. This observation likely relates the chain length dependence of the mechanochemical grafting process.

The presented approach is applicable to particles of varying sizes that span the range of micrometers and nanometers. A superhydrophobic powder with a contact angle larger than 150° can be obtained by using silica particles from 11 nm up to 8 μm in diameter (Figure 2f). The water SA on the superhydrophobic powder has small but noticeable dependence on the size of silica particles used. For nanoscale particles (≤90 nm), the SA is ≈1°. When the particle size increased to microscale dimensions (e.g., 4 μm), the SA increased to ≈7°. Further increasing the particle sizes to 8 μm leads to slight increase of the SA.

2.3. Mechanistic Investigation

The mechanical energy provided by chaotic collisions of balls with the mixed components and the wall of the milling jar enables various physiochemical processes. The ball milling process can induce mechanical mixing of the components leading to either physical adsorption[42,43] or chemical grafting[38] of silicone onto the surface of nanoparticles. Besides that, crystalline to amorphous transition can also take place in the silicon oxide.[44] To confirm whether phase change occurred, we measured the XRD of the samples before and after milling
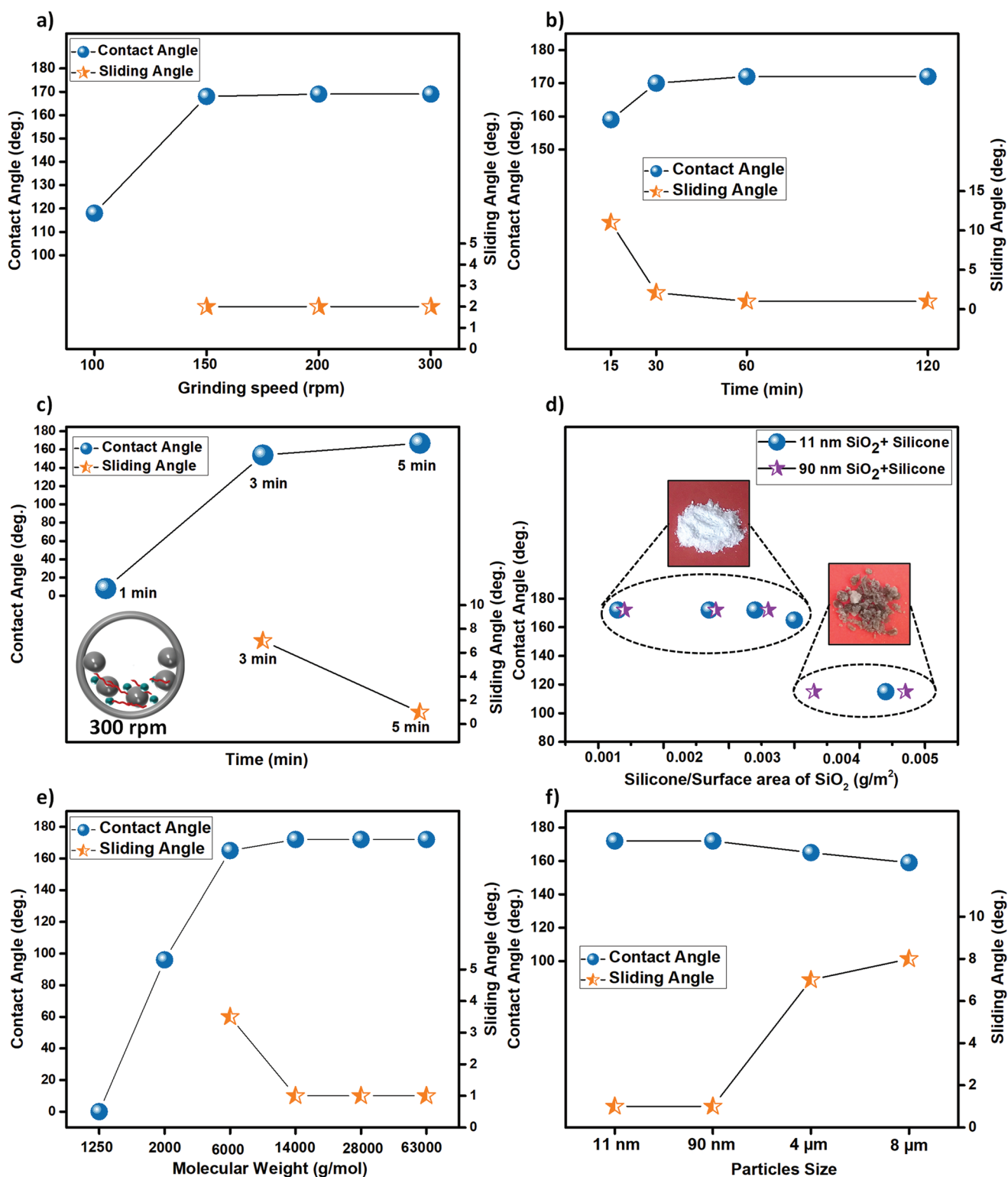
Figure 2. Effects of processing parameters and materials on the surface wetting properties of the powder. a) Effect of the grinding speed on the superhydrophobicity. The grinding time was kept constant at 30 min. b) Variation of water CA (for a droplet of 10 µL) and SA (for a droplet of 5 µL) as a function of the grinding time in ball milling at 200 rpm. c) Effect of the grinding time at a grinding speed of 300 rpm. d) Static CAs of the materials prepared by mixing different ratios of silicone and silica nanoparticles of two different sizes. The horizontal axis was calculated by dividing the amount of silicone to the total surface area (mass × specific surface area) of the nanoparticles. The inset shows the photograph of the resultant powder. e) Effect of the molecular weight of the silicone (1 g) on the water CA and SA of the materials obtained by ball milling with 2 g of silica nanoparticles (11 nm). f) Effect of the diameter of the silica nanoparticles. The molecular weight of the silicone was 63 000 g mol⁻¹ for parts a, b, d, e, and f.

**ADVANCED
SCIENCE NEWS**
www.advancedsciencenews.com

**ADVANCED
MATERIALS
INTERFACES**
Open Access
www.advmatinterfaces.de

(Figure S4, Supporting Information). For silica nanoparticles, a broad XRD peak appears at 2θ angular range between 15° and 30°, confirming amorphous nature of the silica.[45] After ball milling with silicone, a new broad peak appears at $2\theta \approx 11°$ which is due to silicone.[46] The negligible change of the width of silica XRD peak indicates no phase change upon milling.

An effective means of identifying the type of the interaction between silicone and nanoparticles is repeated washing in a solvent. Toluene has been reported for removing ungrafted silicone from planar silicon substrates.[38] We washed the superhydrophobic powder obtained at the end of the ball milling process with toluene under mechanical agitation for 15 min. To ensure complete removal of ungrafted silicone chains, this washing step was repeated for 4 times. The superhydrophobicity was retained following this stringent washing process (see Figure S5, Supporting Information). This observation is a first strong indication of the grafting of silicone to the surface of silica nanoparticles. The same process was carried out in silicone grafted TiO_2. The superhydrophobicity of TiO_2 was retained following this washing process (Figure S5, Supporting Information).

Chemical characterization of the washed sample using XPS and FTIR further confirmed grafting of silicone to the surface of nanoparticles. In the FTIR spectrum (**Figure 3**a), the C—H stretch peaks observed ≈ 2920 and 2850 cm^{-1} shows the presence of silicone molecules even after washing and suggests grafting through the proposed mechanochemical process. Shown in Figure S6 (Supporting Information) is the XPS survey spectra of silica nanoparticles before and after ball milling with silicone, followed by complete washing. The appearance of the C 1s peak at 285.41 eV and elemental composition of $\approx 17.5\%$ indicates the existence of silicone molecules even after complete washing (Figure S6, Supporting Information). The high resolution XPS spectra can help identifying the chemical nature of bonded silicone molecules. The XPS spectrum of silica NPs around Si 2p region is comprised of two overlapping peaks (Figure 3b; also see Table S2, Supporting Information) due to spin orbit coupling (Si $2p_{1/2}$ and $2p_{3/2}$). After grafting, one more peak shows up at the low energy shoulder at 104.0 eV (Figure 3c), which can be assigned to Si—C bond.[47,48] This peak is due to the newly introduced bond (Si—CH3) from the grafted silicone molecules. However, identifying the type of bond formed after grafting becomes ambiguous since the type of chemical bonds before and after reactions is the same. This could be resolved by using TiO_2 NPs (Figure 3d,e). For the superhydrophobic powder obtained from TiO_2 and silicone, a new peak appears at 532.4 eV, at the higher energy side of O 1s peak, indicating formation of Ti—O—Si bond (Figure 3e; also see Table S3, Supporting Information`).[49,50]

To quantify the extent of grafting, TGA was performed. Pristine silica nanoparticles lost weight of 4.4% up to the temperature of 700 °C, corresponding to the desorption of the physically adsorbed molecules (e.g., water) (Figure 3f). In contrast, the ball-milled powder gradually loses weight of 3.9% up to the temperature of 350 °C and then a sharp weight loss (22.4%) from 350 to 650 °C occurs (Figure 3f). The first phase of the weight loss can be attributed to physically adsorbed molecules, water, and silicone molecules. We interpret the weight loss above 350 °C as the decomposition of chemically grafted

silicone molecules.[51,34] This weight loss was used to calculate the degree of grafting.[50,52] The grafting density was calculated to be 0.015 chains nm^{-2} (Scheme S1, Supporting Information). The grafting density is inversely proportional to the MW of silicone, and therefore the calculated grafting density is the lower limit since the rupture of siloxane bonds would lead to lower molecular weight than the one used for the calculation. Here, the grafting density is lower than the values reported in previous studies.[34,50,52]

The results demonstrate the grafting of silicone onto silica NPs. We interpret the results assuming that the silicone chains break under the shear forces in the ball mill (**Figure 4**a,b). Among the possible mechanisms, the hydrolytic scission of siloxane bond ($\equiv$Si—O—) in silicone molecules under the influence of water is well documented.[38] This hydrolytic scission can lead to OH-terminated silicone chains with reduced molecular weight. This OH end group can react slowly, on the order of hours to days, with surface silanol ($\equiv$Si—OH) groups of the NPs via condensation reaction. The control experiments presented in Figure 1b,c show that mechanochemical processing is essential for rapid and effective grafting of silicone resulting in superhydrophobic surfaces in a short time. A recent theoretical study[53] has shown strong coupling between mechanical deformation and hydrolytic chain scission in the backbone of PDMS. The acceleration of the grafting is also possible due to local (a few hundred μm) hot spots that generated upon collision that exceeds 800 °C in temperature and lasts for tens of milliseconds.[54] Another mechanism is the scission of siloxane bond ($\equiv$Si—O—) under mechanical stress induced via ball milling (Figure 4b). Rapture of chemical bonds under mechanical stress has been known for polymers like polystyrene, polymethylmethacrylate,[55] and cellulose[56] and are main reason for mechanical degradation of polymers.[57,58] With respect to the strong siloxane bond, there is only one study that reported bond rapture due to squeezing.[59] Here, the mechanical stress induces elongation along the backbone of siloxane bond, which can eventually lead to bond scission. The most likely pathway is homolytic scission, resulting in the formation of silyl ($\equiv$Si•) and siloxyl (•O-) mechanoradicals.[59] As shown in Figure 4c, the existence of radicals was confirmed via 2,2-diphenyl-1-picrylhydrazyl (DPPH) bleaching test.[59,60] The originally pink ethanolic solution of DPPH becomes pale yellow after getting mixed with the superhydrophobic powder and the UV–vis absorption peak of DPPH at 517 nm decreased (≈ 0.1 absorption unit). Therefore, the mechanism of grafting could involve both hydrolytic and homolytic scission of the siloxane backbone, followed by a reaction between the newly formed OH-terminated silicone chains and radicals with the hydrophilic silica NPs.

2.4. Bulk Superhydrophobicity and Durability

To evaluate practical application potential, a number of tests were conducted. The superhydrophobic powder showed excellent resistance against UV irradiation. There was no noticeable change either in water CA or SA even after UV exposure of 120 h (Figure S7a, Supporting Information). The UV resistance is on par with or better than superhydrophobic coatings reported in recent studies.[61–65] Similarly, the superhydrophobic
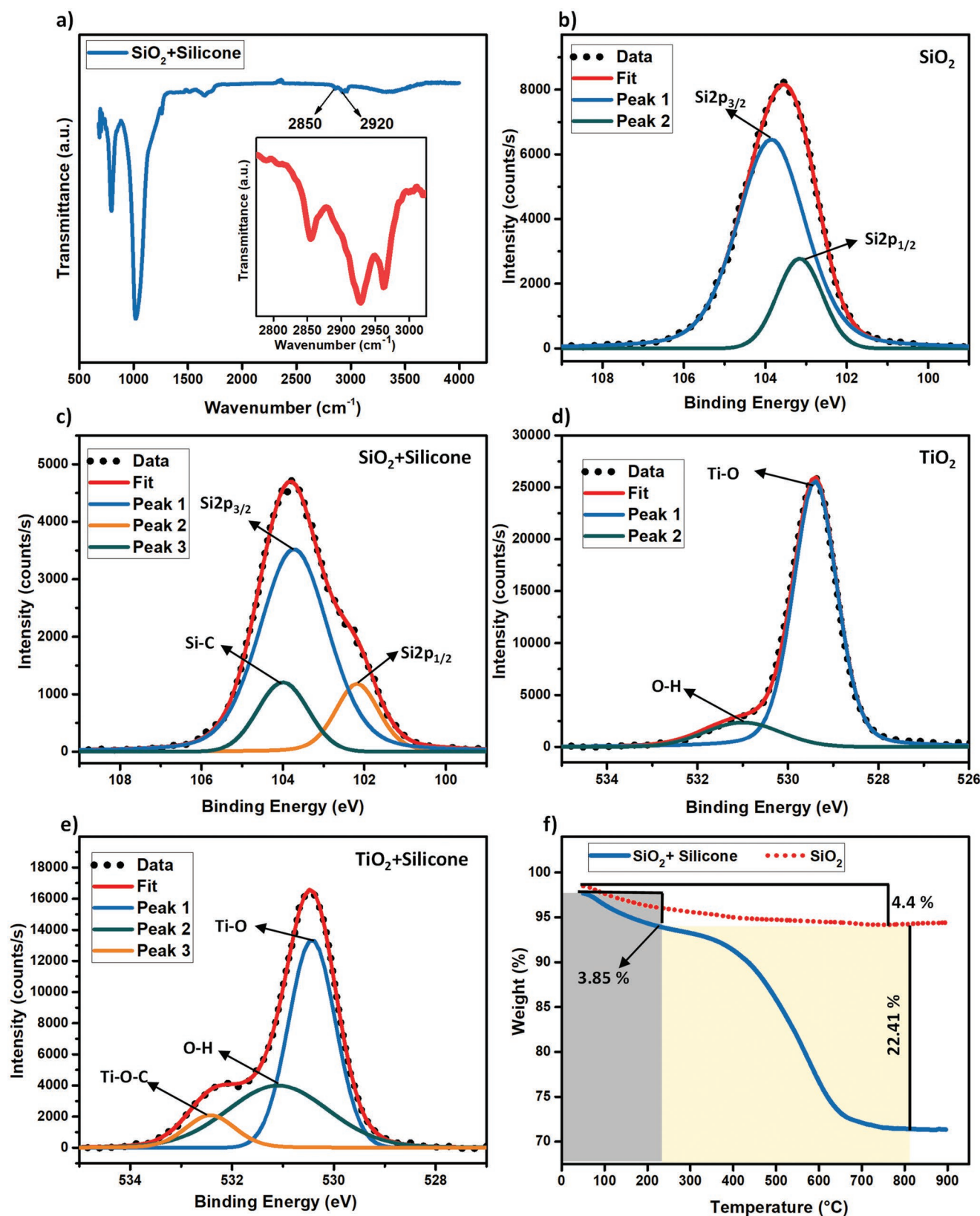
ADVANCED
SCIENCE NEWS

www.advancedsciencenews.com

ADVANCED
MATERIALS
INTERFACES
Open Access
www.advmatinterfaces.de

Figure 3. Grafting of silicone. a) FTIR spectrum of the silicone grafted silica nanoparticles after washing with toluene. The inset shows the range of 2750–3050 cm^{-1}. b–e) High-resolution XPS spectra for (b) bare silica nanoparticles and (c) silicone grafted silica nanoparticles around Si 2p region, and for (d) titania nanoparticles and (e) silicone grafted titania nanoparticles around O 1s region. f) TGA curve of the pristine silica NPs (red dot) and the superhydrophobic powder (blue solid line). The TGA curve of the superhydrophobic powder was obtained after washing 4 times in toluene and drying.
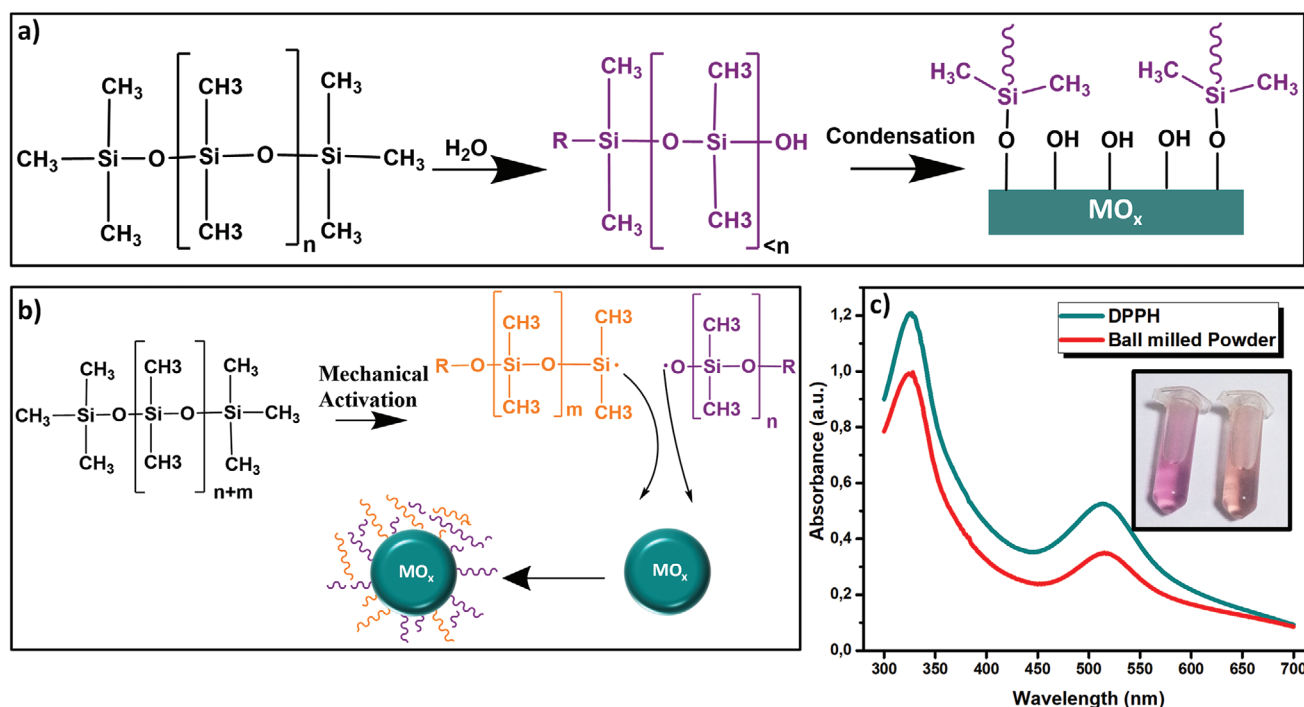
Figure 4. The proposed mechanism of mechanochemical grafting of silicone. a) Schematic illustration of hydrolytic rupture of siloxane bond and subsequent condensation reaction with surface silanol groups. b) Schematic illustration of homolytic scission of the siloxane bond into two radicals and subsequent grafting onto silica NP surface. c) Test of free-radical formation via mechanochemical processing. UV absorbance spectra of DPPH ethanolic solution in the absence and presence of silicone grafted silica nanoparticles. The concentration of DPPH is 5×10^{-6} M. Silicone (63 000 g mol^{-1}) grafted silica nanoparticles with a diameter of 11 nm were added to the solution and mixed for 12 h at 1000 rpm.

powder showed excellent thermal stability, retaining superhydrophobicity at least for 72 h under heating at 200 °C (Figure S7b, Supporting Information). The results of these two tests indicate excellent outdoor durability of the superhydrophobic powder. Another important stability parameter of the superhydrophobic coatings is durability in water and other aqueous solutions that needs to be considered in applications such as food packaging.[66,67] The superhydrophobic powder is stable in acidic (pH 1), neutral, and basic (pH 13) solutions for at least 120 h of immersion (Figure S7c and Video S3, Supporting Information). For comparison, a superhydrophobic coating prepared from very stable polymer PTFE showed CA decrease from 162° to 158° after immersion into an alkaline solution (pH 13) for only 12 h.[65] Another study where a superhydrophobic coating was prepared from PDMS and silica NPs reported slight decrease in CA after immersion into a alkaline solution (pH 14) for 72 h.[64] The pH stability of the superhydrophobic materials presented in this work exceeds previous reports based on silicone grafting.

In addition, the obtained superhydrophobic powders were used to form bulk superhydrophobic monolith and several stability tests were performed to evaluate durability. As shown in **Figure 5**a, a bulk superhydrophobic monolith prepared from the powder could withstand at least 1000 cm of abrasion under a load of 5.26 kPa against a rough sandpaper (180 grit), showing no noticeable change either in water CA or SA. The abrasion resistance is comparable to the state-of-the-art bulk superhydrophobic materials and other robust superhydrophobic coatings.[10,68–72] A knife scratching test also confirmed the stability

against mechanical impact. Even though there was visible damage on the surface of the monolith (Figure 5b), due to the bulk nature of the superhydrophobic monolith, water droplets still bead up even after multiple scratching cycles, retaining superhydrophobicity. In addition, the bulk superhydrophobic monolith showed excellent water impact resistance (Figure 5d) where superhydrophobicity is preserved even after 120 min impact of high-speed water jet (We = 4650). The water jet impact resistance is on par with the latest robust superhydrophobic surfaces.[73,74]

3. Conclusion

The presented mechanochemical approach establishes a practical and sustainable scheme for the formation of superhydrophobic surfaces. The key advantages of this fabrication approach include rapid and completely solvent-free preparation of superhydrophobic materials using widely available and low-cost materials. The process is performed at a single step without additional processing such as centrifugation, filtering, and drying. These advantages stem from versatile mechanochemical grafting of non-functional silicone to particulate materials, overcoming the need for coupling chemistries that require functionalized molecules, tedious separation steps, and excessive usage of solvents. The mechanochemical modification of particulate matter with other hydrophobic agents represent a promising future direction, because of versatile coupling of molecules that are otherwise difficult to associate.
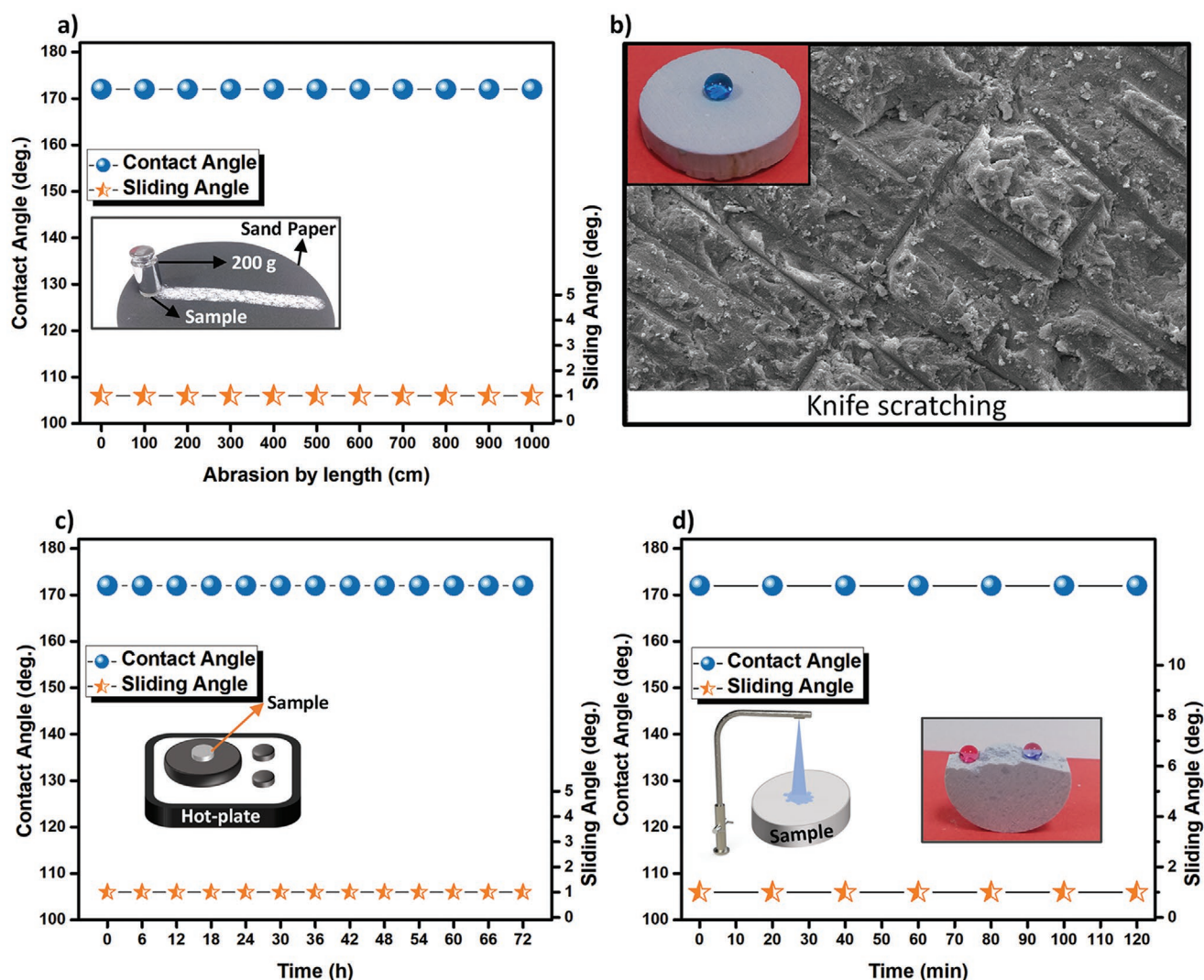
**ADVANCED
SCIENCE NEWS**

www.advancedsciencenews.com

**ADVANCED
MATERIALS
INTERFACES**

Open Access

www.advmatinterfaces.de

Figure 5. Durability of a bulk monolith prepared by pressing the superhydrophobic powder. a) Linear abrasion test. b) Knife scratch test. c) Thermal stability test. d) Water jet impact test.

4. Experimental Section

Silicone (ME-PDMS) with varied molecular weights (1250, 2000, 6000, 14 000, 28 000, and 63 000 g mol^{-1}) were purchased from Alfa Aesar. Silica particles of varied diameter (11 nm, 90 nm, 4 µm, and 8 µm), aluminum oxide (<10 µm), titanium dioxide (21 nm), and zinc oxide (<100 nm) particles were purchased from Sigma–Aldrich. Toluene and DPPH was purchased from Sigma–Aldrich. The L929 (murine fibroblast) cell line was purchased from the American Type Culture Collection (ATCC, Manassas, VA). Cell culture medium Dulbecco's modified Eagle's medium (DMEM) was obtained from the Sigma Chemical Company (St. Louis, USA). SYTO 9 and propidium iodide (PI) nucleic acid dyes were purchased from Thermo Fisher Scientific.

Mechanochemical Grafting of Silicone: Ball milling was carried out in a planetary ball mill (Fritsch, Pulverisette 6) using a 250 mL tungsten carbide (WC) grinding jar. Specifically, 2 g of SiO$_2$ nanoparticles and 1 g of silicone were added to the grinding jar in air, followed by adding 20 WC balls (diameter 10 mm, weight 7.85 g). Then, the device was programed to run at 200 rpm for 30 min, adhering to the cyclic protocol of running clockwise for 3 min, anticlockwise for 3 min while resting for 1 min in between. Besides silica, particles (2 g) of various compositions (TiO$_2$, ZnO, Al$_2$O$_3$) can also be ball milled with silicone

(0.25 g) to impart superhydrophobicity. Unless stated otherwise, silica nanoparticles of 11 nm in size and silicone of 63 000 g mol^{-1} molecular weight were used. For various measurements, the obtained powder was retrieved using a spatula.

Grafting without Ball Milling: To study the effect of ball milling on the grafting of silicone, control experiments in the absence of mechanochemical processing were performed. The grafting was performed at room temperature and at 100 °C following a procedure as described in a previous study.[38] Specifically, silicone (63 000 g mol^{-1}) was spread on the surface of a petri dish, followed by adding 2 g of SiO$_2$ nanoparticles (11 nm). To ensure full coverage of the surface of the particles, another layer of silicone (63 000 g mol^{-1}) was poured on the surface. These samples were treated for 30 min and 24 h at room temperature and 100 °C.

Characterization: The wetting properties of samples were measured using an optical tensiometer (Attension, Theta Lite). The CA and SA were measured on at least three different spots using water droplets of 10 and 5 µL, respectively. The deviation of CA is ≈2° and for SA it is ≈1°. The CA and SA of powders obtained via grafting were measured after complete removal of ungrafted silicone via washing in toluene for four times, 15 min each. Then, the powder was placed on a flat surface and flattened using a glass slide, followed by measuring the wetting properties as mentioned earlier.

2300069 (9 of 12)

X-ray photoelectron spectroscopy (XPS) was used to decern any chemical changes. Specifically, after ball milling, a certain amount of superhydrophobic powder was retrieved, thoroughly washed with toluene to remove any unreacted silicone molecules, followed by drying the samples at 80 °C for 12 h. Then, the XPS data were taken in an ultrahigh vacuum using a Thermo Scientific K-Alpha X-ray photoelectron spectrometer. For the XPS measurement, a monochromatic Al Kα X-ray source (1486.7 eV, 6 mA) incident upon the samples at an angle of 30°, and the emitted electrons were collected at 60° and detected with a hemispherical electron energy analyzer. The survey scan spectra were measured at a pass energy of 200 eV with a step size of 1 eV while the high-resolution scans were recorded at a pass energy of 30 eV with a step size of 0.1 eV. The spot radius of the X-ray beam was 400 μm. During the measurements, a flood gun was used for charge compensation. The XPS data were calibrated against C 1s peak at 284.8 eV. Curve fitting of XPS data was performed using open-source Python packages RamPy and lmfit. Thermogravimetric analysis (TGA) was measured using Q500 (TA instrument) by loading samples (5–10 mg) onto an aluminum pan. The sample was heated under the flow of nitrogen gas (60 mL min^{-1}) with a temperature ramp of 10 C°min^{-1}.

To observe whether radicals were generated during the ball milling process, a radical scavenging test was conducted using DPPH. This molecule is a stable free radical with a strong UV–vis absorption at 520 nm that appears violet. DPPH has strong tendency to react with other radicals and be consumed, upon which it becomes colorless or pale yellow. For radical scavenging tests, 1.0 g of the milled sample was immediately retrieved from the grinding jar and added to a test tube containing a 20 mL ethanolic solution (5×10^{-5} mol) of the radical scavenger DPPH, followed by mixing for 12 h. In the end, the test tube was centrifuged at 4000 rpm for 15 min to sediment the particles and 20 mL of solution was withdrawn from the top. The pink color of the original solution becomes pale yellow, indicating the existence of radicals in the milled superhydrophobic powder, which was further confirmed by UV–vis measurement.[59,60]

Monolith Fabrication and Durability Tests: Several tests were performed to evaluate the durability of a monolith prepared from the superhydrophobic powder. Specifically, the monolith was prepared by pressing 4.0 g of the superhydrophobic powder in a cylindrical mold under the load of 1500 kg at room temperature. The obtained monolith is a cylindrical plate with a radius of 11 mm and height of 5 mm. Resistance against wear was evaluated by abrading the monolith against a sandpaper with a grit size of 180 under the weight of a 200 g object (load ≈5.26 kPa), followed by measuring water CA and SA after each 100 cm of linear abrasion. Scratch resistance was evaluated by scratching the monolith surface with a sharp steel knife several times. Thermal stability was evaluated by heating the monolith on a heat plate at 200 °C in atmospheric conditions for 6 h, followed by measuring the water CA and SA after the monolith was allowed to naturally cool down to room temperature. This process was repeated for 12 times (72 h in total) to evaluate long term thermal stability. Durability against water impact was tested by placing the monolith (30° horizontal) under the impact (28.0 kPa) of water jet coming out of a faucet with inner opening diameter of 5.8 mm with a flow rate of ≈0.2 L s^{-1} (average velocity = 7.6 m s^{-1}, Weber number We = 4650). The water CA and SA values were measured after 20 min of water jet impact and repeated for six times (120 min in total). The stability of the superhydrophobic powder was also investigated. To examine the chemical resistance of the powder, the powder was kept in pure water, pH 1 and 13 solutions for 120 h. To determine the resistance of the powder to UV light, the sample was exposed to a light source with a wavelength of 254 nm for 120 h. The distance between the powder and the UV light source was set to 3 cm. To examine the thermal resistance of the powder, the powder was heated for 72 h at 200 °C.

Cell Culture: L929 Cells were cultured in DMEM supplemented with 10% fetal bovine serum (FBS), 1% penicillin/streptomycin, and 1% glutamine at 37 °C in a humidified atmosphere of 5% CO$_2$. SYTO 9 and PI nucleic acid dyes dissolved in dimethyl sulfoxide at a concentration of 3.34 and 20 mM, respectively.

Cytotoxicity Test: L929 cell line was chosen according to ISO10993-5-2009 regulation. The MTT assay, a colorimetric method, was used for evaluation of cell viability. Ten milligrams superhydrophobic samples ($n = 3$) were sterilized for 40 min and 1 mL of complete medium was added to each. The dispersion was vortexed for 10 s to increase the interaction of the samples with the medium. The dispersion was then placed in 96-well tissue culture plates and incubated for 24 h in 5% CO$_2$ at 37 °C. Under the same conditions and simultaneously, L929 cells were incubated in 100 μL culture medium at an initial density of 6×10^3 cells per well in 96-well culture plates. The cell number was determined by manually counting a 0.4% trypan blue-stained cell suspension using a hemocytometer. After the incubation, the medium-sample mixture was filtered through filters with a pore diameter of 0.20 μm and extraction solutions (10 mg mL^{-1}) were obtained. After that, 100 μL of cell culture medium was changed with this extraction medium and incubated for 24 h. After the incubation, the general morphology of the cells was evaluated microscopically. For viability analysis afterward, the cells were incubated with 10 μL of 3-(4,5-dimethylthiazol-2-yl)-2,5-diphenyltetrazolium bromide solution (MTT, 5 mg mL^{-1}, Sigma–Aldrich, Germany) for 3 h, formazan crystals were dissolved in 100 μL of dimethyl sulfoxide. Cell viability was calculated using the equation below by measuring absorbance values at 560 nm with a microplate reader (Promega Multireader Glomax, USA):

$$\text{Cell viability \%} = \frac{\text{ODsample}}{\text{ODcontrol}} \times 100\% \tag{1}$$

Experiments were performed in triplicate and mean OD values were normalized to control group and represented as cell viability (%). Each experiment is given as the average of the studies performed in 3 replicates and at 3 different times.

For the fluorescent live/dead cell assay (SYTO 9 and PI kit), trypsin solution was added to the cell culture incubated with the extraction medium, and the cells were detached after 2–3 min of incubation. Complete medium was added to inactivate trypsin and cells were suspended. The cell suspension was then transferred to an Eppendorf tube and gently centrifuged at 300 g for 5 min. After removing the supernatant, the cell pellet was gently resuspended in 0.85% NaCl solution. This washing process was repeated 3 times in order to thoroughly remove the medium residues in the suspension. After that, 3 μL of SYTO 9 (diluted to 1 mM in dH$_2$O) and 1 μL of PI (diluted to 2 mM in dH$_2$O) were added to 100 μL of cell suspension (2×10^5 cells) and incubated for 15 min at room temperature in the dark. After incubation, 10 μL of the stained cell suspension was pipetted onto a glass slide and fluorescence microscope images were taken using by a ZEISS Axio Imager 2 microscope.

Statistical Analysis: Statistical significance between groups was analyzed using one-way analysis of variance (ANOVA) followed by Tamhane T2 post-hoc test. Significance was accepted at a p-value of <0.05 using the SPSS 21.0 (IBM, USA). The results are expressed as the mean ± standard deviation (SD) of three independent assays. Live/dead cell counts from fluorescent images were performed using ImageJ.

Supporting Information

Supporting Information is available from the Wiley Online Library or from the author.

Acknowledgements

ADVANCED
SCIENCE NEWS
www.advancedsciencenews.com

ADVANCED
MATERIALS
INTERFACES
Open Access
www.advmatinterfaces.de

[1] A. Lafuma, D. Quéré, *Nat. Mater.* **2003**, *2*, 457.
[2] L. Gao, T. J. McCarthy, *Langmuir* **2009**, *25*, 14105.
[3] F. Geyer, M. D'Acunzi, A. Sharifi-Aghili, A. Saal, N. Gao, A. Kaltbeitzel, T.-F. Sloot, R. Berger, H.-J. Butt, D. Vollmer, *Sci. Adv.* **2020**, *6*, eaaw9727.
[4] W. Barthlott, C. Neinhuis, *Planta* **1997**, *202*, 1.
[5] B. Bhushan, Y. C. Jung, *Prog. Mater. Sci.* **2011**, *56*, 1.
[6] X. Tian, S. Shaw, K. R. Lind, L. Cademartiri, *Adv. Mater.* **2016**, *28*, 3677.
[7] I. Torun, N. Celik, M. Hancer, F. Es, C. Emir, R. Turan, M. S. Onses, *Macromolecules* **2018**, *51*, 10011.
[8] T. Zhu, Y. Cheng, J. Huang, J. Xiong, M. Ge, J. Mao, Z. Liu, X. Dong, Z. Chen, Y. Lai, *Chem. Eng. J.* **2020**, *399*, 125746.
[9] S. M. Gateman, K. Page, I. Halimi, A. R. C. Nascimento, S. Savoie, R. Schulz, C. Moreau, I. P. Parkin, J. Mauzeroll, *ACS Appl. Mater. Interfaces* **2020**, *12*, 1523.
[10] M. J. Nine, M. A. Cole, L. Johnson, D. N. H. Tran, D. Losic, *ACS Appl. Mater. Interfaces* **2015**, *7*, 28482.
[11] L. Wang, Q. Gong, S. Zhan, L. Jiang, Y. Zheng, *Adv. Mater.* **2016**, *28*, 7729.
[12] R. Liao, Z. Zuo, C. Guo, Y. Yuan, A. Zhuang, *Appl. Surf. Sci.* **2014**, *317*, 701.
[13] A. K. Kota, G. Kwon, W. Choi, J. M. Mabry, A. Tuteja, *Nat. Commun.* **2012**, *3*, 1025.
[14] X. Gao, J. Zhou, R. Du, Z. Xie, S. Deng, R. Liu, Z. Liu, J. Zhang, *Adv. Mater.* **2016**, *28*, 168.
[15] L. Kang, B. Wang, J. Zeng, Z. Cheng, J. Li, J. Xu, W. Gao, K. Chen, *Green Chem.* **2020**, *22*, 504.
[16] J. Liu, L. Ye, Y. Sun, M. Hu, F. Chen, S. Wegner, V. Mailänder, W. Steffen, M. Kappl, H. Butt, *Adv. Mater.* **2020**, *32*, 1908008.
[17] H. Zhong, Z. Zhu, J. Lin, C. F. Cheung, V. L. Lu, F. Yan, C.-Y. Chan, G. Li, *ACS Nano* **2020**, *14*, 6213.
[18] F. Geyer, M. D'Acunzi, C.-Y. Yang, M. Müller, P. Baumli, A. Kaltbeitzel, V. Mailänder, N. Encinas, D. Vollmer, H.-J. Butt, *Adv. Mater.* **2019**, *31*, 1801324.
[19] H. Han, J. S. Lee, H. Kim, S. Shin, J. Lee, J. Kim, X. Hou, S. W. Cho, J. Seo, T. Lee, *ACS Nano* **2018**, *12*, 932.
[20] S. Pekdemir, I. Torun, M. Sakir, M. Ruzi, J. A. Rogers, M. S. Onses, *ACS Nano* **2020**, *14*, 8276.
[21] M. Eriksson, M. Tuominen, M. Järn, P. M. Claesson, V. Wallqvist, H.-J. Butt, D. Vollmer, M. Kappl, J. Schoelkopf, P. A. C. Gane, H. Teisala, A. Swerin, *ACS Nano* **2019**, *13*, 2246.
[22] N. Celik, I. Torun, M. Ruzi, A. Esidir, M. S. Onses, *Chem. Eng. J.* **2020**, *396*, 125230.
[23] L. Zhai, F. C. Cebeci, R. E. Cohen, M. F. Rubner, *Nano Lett.* **2004**, *4*, 1349.
[24] N. Wang, D. Xiong, Y. Deng, Y. Shi, K. Wang, *ACS Appl. Mater. Interfaces* **2015**, *7*, 6260.
[25] Y. Chen, H. Liu, L. Yu, Q. Duan, Z. Ji, L. Chen, *ACS Sustain. Chem. Eng.* **2020**, *8*, 10423.
[26] E. M. Sunderland, X. C. Hu, C. Dassuncao, A. K. Tokranov, C. C. Wagner, J. G. Allen, *J. Expo. Sci. Environ. Epidemiol.* **2019**, *29*, 131.
[27] D. Prat, A. Wells, J. Hayler, H. Sneddon, C. R. McElroy, S. Abou-Shehada, P. J. Dunn, *Green Chem.* **2015**, *18*, 288.
[28] I. S. Bayer, A. J. Davis, E. Loth, A. Steele, *Mater. Today Commun.* **2015**, *3*, 57.
[29] L. Xiao, W. Zeng, G. Liao, C. Yi, Z. Xu, *ACS Appl. Nano Mater.* **2018**, *1*, 1204.
[30] S. Liu, X. Zhang, S. Seeger, *ACS Appl. Mater. Interfaces* **2019**, *11*, 44691.
[31] L. Shen, H. Ding, Q. Cao, W. Jia, W. Wang, Q. Guo, *Carbon* **2012**, *50*, 4284.
[32] L. R. J. Scarratt, B. S. Hoatson, E. S. Wood, B. S. Hawkett, C. Neto, *ACS Appl. Mater. Interfaces* **2016**, *8*, 6743.
[33] S. Kim, J. W. Lee, W. Hwang, *ACS Appl. Mater. Interfaces* **2020**, *12*, 28869.
[34] A. P. Amrute, B. Zibrowius, F. Schüth, *Chem. Mater.* **2020**, *32*, 4699.
[35] J. L. Do, T. Friščić, *ACS Cent. Sci.* **2017**, *3*, 13.
[36] A. S. Heintz, M. J. Fink, B. S. Mitchell, *Adv. Mater.* **2007**, *19*, 3984.
[37] J. W. Krumpfer, T. J. McCarthy, *Langmuir* **2011**, *27*, 11514.
[38] H. Teisala, P. Baumli, S. A. L. Weber, D. Vollmer, H.-J. Butt, *Langmuir* **2020**, *36*, 4416.
[39] M. Rezaei, P. Radfar, M. Winter, L. McClements, B. Thierry, M. E. Warkiani, *Anal. Chem.* **2021**, *93*, 4584.
[40] N. Celik, F. Sahin, S. S. Ozel, G. Sezer, N. Gunaltay, M. Ruzi, M. S. Onses, *Langmuir* **2023**, *39*, 3194.
[41] T. G. Deligeorgiev, S. Kaloyanova, J. J. Vaquero, *Recent Pat. Mater. Sci.* **2009**, *2*, 1.
[42] V. M. Litvinov, H. Barthel, J. Weis, *Macromolecules* **2002**, *35*, 4356.
[43] P. A. Klonos, L. V. Nosach, E. F. Voronin, E. M. Pakhlov, A. Kyritsis, P. Pissis, *J. Phys. Chem. C* **2019**, *123*, 28427.
[44] K. Gobindlal, Z. Zujovic, P. Yadav, J. Sperry, C. C. Weber, *J. Phys. Chem. C* **2021**, *125*, 20877.
[45] R. K. Biswas, P. Khan, S. Mukherjee, A. K. Mukhopadhyay, J. Ghosh, K. Muraleedharan, *J. Non-Cryst. Solids* **2018**, *488*, 1.
[46] J. J. H. Lancastre, N. Fernandes, F. M. A. Margaça, I. M. Miranda Salvado, L. M. Ferreira, A. N. Falcão, M. H. Casimiro, *Radiat. Phys. Chem.* **2012**, *81*, 1336.
[47] M. R. Alexander, R. D. Short, F. R. Jones, W. Michaeli, C. J. Blomfield, *Appl. Surf. Sci.* **1999**, *137*, 179.
[48] E. McCafferty, J. P. Wightman, *Surf. Interface Anal.* **1998**, *26*, 549.
[49] B. Erdem, R. A. Hunsicker, G. W. Simmons, E. D. Sudol, V. L. Dimonie, M. S. El-Aasser, *Langmuir* **2001**, *17*, 2664.
[50] S. Wooh, N. Encinas, D. Vollmer, H.-J. Butt, *Adv. Mater.* **2017**, *29*, 1604637.
[51] R. Mueller, H. K. Kammler, K. Wegner, S. E. Pratsinis, *Langmuir* **2003**, *19*, 160.
[52] J. Lin, H. Chen, Y. Yuan, Y. Ji, *Appl. Surf. Sci.* **2011**, *257*, 9024.
[53] M. P. Kroonblawd, N. Goldman, J. P. Lewicki, *J. Phys. Chem. B* **2019**, *123*, 7926.

[54] A. W. Tricker, G. Samaras, K. L. Hebisch, M. J. Realff, C. Sievers, *Chem. Eng. J.* **2020**, *382*, 122954.

[55] G. I. Peterson, W. Ko, Y.-J. Hwang, T.-L. Choi, *Macromolecules* **2020**, *53*, 7795.

[56] Ö. Laçin, J. Kwiczak-Yiğitbaşı, M. Erkan, Ş. C. Cevher, B. Baytekin, *Polym. Degrad. Stab.* **2019**, *168*, 108945.

[57] G. Gorrasi, A. Sorrentino, *Green Chem.* **2015**, *17*, 2610.

[58] M. K. Beyer, H. Clausen-Schaumann, *Chem. Rev.* **2005**, *105*, 2921.

[59] H. T. Baytekin, B. Baytekin, B. A. Grzybowski, *Angew. Chem., Int. Ed.* **2012**, *51*, 3596.

[60] O. Cocco, S. Garroni, S. Enzo, G. Pia, P. Meloni, F. Delogu, *J. Phys. Chem. C* **2018**, *122*, 2773.

[61] Z. Liu, C. Zhang, X. Zhang, C. Wang, F. Liu, R. Yuan, H. Wang, *Chem. Eng. J.* **2021**, *411*, 128632.

[62] W. S. Y. Wong, Z. H. Stachurski, D. R. Nisbet, A. Tricoli, *ACS Appl. Mater. Interfaces* **2016**, *8*, 13615.

[63] J. Huang, S. Lyu, Z. Chen, S. Wang, F. Fu, *J. Colloid Interface Sci.* **2019**, *536*, 349.

[64] X. Gong, S. He, *ACS Omega* **2020**, *5*, 4100.

[65] J. Huang, M. Yang, H. Zhang, J. Zhu, *ACS Appl. Mater. Interfaces* **2021**, *13*, 1323.

[66] M. Ruzi, N. Celik, M. S. Onses, *Food Packag. Shelf Life* **2022**, *32*, 100823.

[67] F. Sahin, N. Celik, A. Ceylan, S. Pekdemir, M. Ruzi, M. S. Onses, *Chem. Eng. J.* **2022**, *431*, 133445.

[68] Z. Dong, M. Vuckovac, W. Cui, Q. Zhou, R. H. A. Ras, P. A. Levkin, *Adv. Mater.* **2021**, *33*, 2106068.

[69] G. Kaur, A. Marmur, S. Magdassi, *Addit. Manuf.* **2020**, *36*, 101669.

[70] W. Zhang, T. Xiang, F. Liu, M. Zhang, W. Gan, X. Zhai, X. Di, Y. Wang, G. Liu, C. Wang, *ACS Appl. Mater. Interfaces* **2017**, *9*, 15776.

[71] A. Davis, S. Surdo, G. Caputo, I. S. Bayer, A. Athanassiou, *ACS Appl. Mater. Interfaces* **2018**, *10*, 2907.

[72] S. Liu, W. Wan, X. Zhang, A. De Crema, S. Seeger, *Chem. Eng. J.* **2020**, *385*, 123969.

[73] D. Wang, Q. Sun, M. J. Hokkanen, C. Zhang, F.-Y. Lin, Q. Liu, S.-P. Zhu, T. Zhou, Q. Chang, B. He, Q. Zhou, L. Chen, Z. Wang, R. H. A. Ras, X. Deng, *Nature* **2020**, *582*, 55.

[74] C.-H. Xue, H.-D. Wang, Z.-Y. Ji, X.-J. Guo, B.-Y. Liu, Y. Wu, S.-T. Jia, *ACS Omega* **2019**, *4*, 19756.

2300069 (12 of 12)